Bone 190 (2025) 117288

Contents lists available at ScienceDirect

Bone

journal homepage: www.elsevier.com/locate/bone

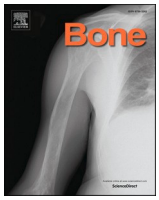

Full Length Article

OMIBONE: Omics-driven computer model of bone regeneration for personalized treatment

Mahdi Jaber [a], Johannes Schmidt [b], Stefan Kalkhof [b], Louis Gerstenfeld [c], Georg N. Duda [a,d], Sara Checa [a,*]

[a] Julius Wolff Institute, Berlin Institute of Health at Charité – Universitätsmedizin Berlin, Germany
[b] Department of Preclinical Development and Validation, Fraunhofer Institute for Cell Therapy and Immunology, Leipzig, Germany
[c] Department of Orthopaedic Surgery, Boston University of Medicine, Boston, MA, United States of America
[d] BIH Center for Regenerative Therapies, Berlin Institute of Health at Charité, Universitätsmedizin Berlin, Germany

ARTICLE INFO

Keywords:
Proteomics
Computational modeling
Bone regeneration
Personalized treatment
Ingenuity Pathway Analysis (IPA)
Agent Based Model (ABM)

ABSTRACT

Treatment of bone fractures are standardized according to the AO classification, which mainly refers to the mechanical stabilization required in a given situation but neglect individual differences due to patient's healing potential or accompanying diseases. Specially in elderly or immune-compromised patients, the complexity of individual constrains on a biological as well as mechanical level are hard to account for. Here, we introduce a novel framework that allows to predict bone regeneration outcome using combined proteomic and mechanical analyses in a computer model. The framework uses Ingenuity Pathway Analysis (IPA) software to link protein changes to alterations in biological processes and integrates these in an Agent-Based Model (ABM) of bone regeneration. This combined framework allows to predict bone formation and the potential of an individual to heal a given fracture setting. The performance of the framework was evaluated by replicating the experimental setup of a mouse femur fracture stabilized with an intramedullary pin. The model was informed by serum derived proteomics data. The tissue formation patterns were compared against experimental data based on x-ray and histology images. The results indicate the framework potential in predicting an individual's bone formation potential and hold promise as a concept to enable personalized bone healing predictions for a chosen fracture fixation.

1. Introduction

Bone regeneration is a remarkable natural process facilitating the scar-free restoration of bone tissue following injury. However, current approaches in the treatment of bone fractures mainly rely on the standardized AO classification system which takes into account the anatomical characteristics of fractures, patient physiology, and medical history [1] and adheres to a standardized method for all patients. Such approaches are particularly beneficial for assigning fixators based on fracture type, through accurate visualization of bone fractures, assessment of soft tissue injuries associated with fractures as well as identification of risk factors. However, they overlook the complex individual variations in healing attributes. Traditionally, therapies have been tailored to the 'average patient,' disregarding the innate variations present among individuals [2]. This presents a significant clinical challenge, as responses to standardized treatments can vary among different individuals [3], leading to suboptimal results and possible complications. Moreover, these clinical measures fall short in quantifying the underlying biological processes associated with the healing progression or identifying individuals at risk for nonunion development. Consequently, there exists an urgent need towards novel strategies that account for the distinct healing potential of each patient [4,5], thus enhancing the outcomes of bone regeneration.

With the rise of high-throughput and data-intensive approaches in the recent years [4], omics technologies have emerged as powerful tools to address the challenge of patient-specific bone regeneration. These technologies offer comprehensive insights into the molecular profiles of individual patients, providing a holistic view about their genetic makeup, gene expression dynamics and protein characteristics. Proteomics, a subfield of omics, allows for the systematic study of the complete set of proteins expressed by cells, and found in many tissues and various bio-fluids. These proteins are the primary effectors of cellular

* Corresponding author at: Julius Wolff Institute, Berlin Institute of Health at Charité, Universitätsmedizin Berlin, Augustenburger Platz 1, 13353 Berlin, Germany.
E-mail address: sara.checa@charite.de (S. Checa).

https://doi.org/10.1016/j.bone.2024.117288
Received 13 May 2024; Received in revised form 2 October 2024; Accepted 13 October 2024
Available online 18 October 2024

functions, including those involved in bone regeneration. In addition, proteomics captures post-translational modifications that significantly influence protein function and cellular processes [6]. Although proteomics analyses have been extensively used to investigate different tissues, such as epithelial [7–9], muscle [10,11], connective [12,13] and nervous tissues [14,15] and different diseases, such as diabetes [16–18], cancer [19–21], and heart disease [22–24], their application to bone regeneration is in its infancy [25–28].

To date, only a few studies have focused on the assessment of the proteomics profile during the process of bone regeneration. Boteanu et al. used proteomics analyses to evaluate the effect of a titanium implant coated with a PEG biopolymer for gradual delivery of growth factors (FGF2, VEGF, and BMP4) in a rat diaphyseal in vivo tibial defect model. They identified common but also unique proteins actively involved in the new tissue regeneration located at the interface of each implant with the bone defect [25]. For example, a high abundance of GC (vitamin D-binding protein) was detected in the FGF2/VEGF/BMP4 group after 6 weeks which was correlated with ceruloplastamin, the primary copper transporting protein involved in the wound healing process [25]. Calciolari et al. showed that osteoporotic rats with calvarial critical size defects had upregulated inflammatory and stress pathways, which resulted in delayed osseous maturation and reduced bone formation [26]. Using wound fluid from a rat defect model, Förster et al. demonstrated that proteins involved in early immune response, such as neutrophil chemoattractants, showed increased levels in bone defects than in soft tissue wounds [29]. In a recent review, Calciolari and Donos described how proteomics can help elucidating molecular processes involved in bone regeneration in healthy and diseased conditions. They suggested that such approaches can improve the quality of regeneration outcomes, particularly in patients with chronic diseases like diabetes and osteoporosis [30].

Computer models of bone regeneration have the potential to tailor treatments to individual patients, improve clinical decision-making, reduce costs, and enhance patient outcomes. Previously developed and validated computer models [31–33] have been instrumental in predicting bone healing outcomes in in vivo pre-clinical experiments. These models simulate tissue formation dynamics, coupling both mechanical and biological characteristics to predict the distribution patterns of tissues within a healing volume over time. Such models have the capacity to capture the effect of biomechanical differences on bone healing such as in different fixators [31], different implants [34,35] or even in different bone characteristics [33]. Moreover, these models were able to simulate altered healing in biologically compromised conditions such as in Type 2 diabetes and ageing [31,33]. However, they do not consider the individual patient's unique molecular characteristics that vary across the population. Therefore, there is a need for computer models that consider patient's unique healing capacity, where it becomes possible to tailor predictions to each patient's specific intrinsic regenerative capacity. Such computer models will not only have the capacity to qualitatively assess the healing progression but also to capture the underlying biological mechanisms that resulted in the healing outcome.

Therefore, the primary aim of this study was to develop a novel computer model of bone regeneration that incorporates patient-specific omics data to predict personalized healing outcomes considering the biomechanical constrains imposed by the fixation system. To achieve this aim, we introduce a comprehensive framework that combines proteomic and mechanical analyses in computational modeling, facilitating predictions of bone regeneration outcomes. This framework, termed OMIBONE (OMIcs-driven computer model of BOne regeNEration for personalized treatment) extends upon a previously validated computer model of bone regeneration [32] to integrate proteomics data. The framework of OMIBONE employs the Ingenuity Pathway Analysis (IPA) software to perform a Downstream Effects Analysis and derive relationships between the up and down regulation of proteins and their effect on cellular function. To validate the predictive capabilities of the framework, OMIBONE was tested for its predictive ability to simulate bone healing progression in a mouse fractured femur stabilized with an intramedullary pin [27]. Computer model predictions of the bone healing progression were compared to histological and x-ray images at several time points during the bone healing process.

2. Material and methods

In this section, the general methodology employed to integrate omics data into a computer model of bone regeneration is first described. Thereafter, the specific implementation of the model to simulate bone fracture healing in a mouse model is presented.

2.1. Baseline computer model of bone regeneration

A previously described and experimentally validated bone regeneration computer model was used as a baseline model [32]. The computer model combined finite element (FE) analysis, to determine the mechanical environment within the healing region, and an agent-based model (ABM) describing the biological processes taking place during bone regeneration at the cellular level [32]. In this section, the baseline model will be briefly described.

A finite element model is used to quantify the mechanical environment within the healing region. This model considers the mechanical stability provided by the fixation system and the load sharing between the callus and the specific fixator. Moreover, a callus region is modeled around the fracture gap, where the mechanical environment is iteratively determined during the healing process. These mechanical stimuli determined by the FE model are then used as inputs to a coupled agent-based computer model to simulate various activities that happen in the cellular level during bone healing. In the healing region (callus), a 3D grid is embedded, where each of the grid positions represents a potential space a cell could occupy. Different cell phenotypes are simulated (e.g. mesenchymal cells (MSC), fibroblasts, chondrocytes, immature osteoblasts and mature osteoblasts), with cell-phenotype specific cellular activity rates. The model simulates cellular processes including migration, proliferation, differentiation and apoptosis. The local mechanical stimuli, as determined by the FE model, influence the differentiation of MSCs into osteoblasts, chondrocytes, or fibroblasts, as informed by previous work [36].

To simulate the invasion of MSCs from the marrow cavity and periosteum, 30 % of the grid positions along the periosteum and marrow cavity are initially seeded with MSCs [32]. Cells are simulated to produce the corresponding extracellular matrix (osteoblasts: bone, chondrocytes: cartilage and fibroblasts: fibrous tissue), that is implemented as a change in the mechanical properties of the tissue in the FE model. Each element property is then determined using a rule of mixtures to account for different tissues being present in the same element [37]. In addition, each element property is averaged over the last ten iterations to account for the delay in actual ECM maturation [38].

2.2. Integration of proteomics – OMIBONE framework

The baseline computer model of bone regeneration was further developed to incorporate proteomics data [32]. A systematic approach was developed to translate proteomics data into cellular activity rates in the ABM. In general, the framework uses the software Ingenuity Pathway Analysis tool (IPA, QIAGEN Redwood City) to derive a statistical score of the role of differentially expressed proteins on specific cellular functions. Thereafter, this score is used to scale cellular activity rates during the bone healing simulation (Fig. 1).

For the given set of differentially expressed proteins, a downstream effects analysis is performed using the software Ingenuity Pathway Analysis tool (IPA, QIAGEN Redwood City). In this analysis, a statistical score is determined which indicates the relevance of each specific protein change on biological functions (e.g. cell migration, differentiation). This statistical score is based on software knowledge from an extensive

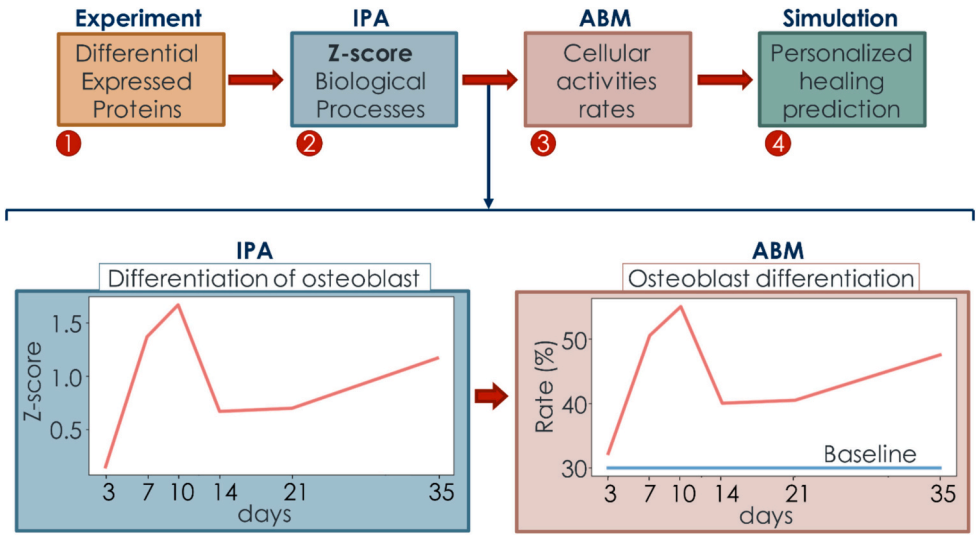

Fig. 1. OMIBONE framework: from proteomics data to prediction of tissue formation during the regeneration process, IPA's z-score of biological processes is mapped to cellular activity rates in an agent-based model of bone regeneration.

literature data collection. The statistical score, named z-score, refers to the activation/inhibition of a biological process, where a positive score indicates activation and a negative score indicates inhibition. In this study, we focus on biological processes similar to the ones existing in the ABM of the baseline computer model of bone regeneration, as shown in Table 1.

Thereafter, the rates of the cellular activities in the ABM are determined according to the z-score of each biological process given by IPA. The mapping approach of the z-score of the biological processes to the cellular activity rates should ensure that the influence of biological processes on cellular activities is reflected proportionally, i.e. higher z-scores correspond to higher cellular activity rates, and lower z-scores correspond to lower rates. Therefore, 1D linear transformation (linear scaling) was done to map the z-score of each biological process obtained from IPA to the cellular activity rates in the ABM (Fig. 1). The mapping was performed using the following linear equation:

$$Y(z) = BS + z \times k(BS) \tag{1}$$

where Y is the mapped cellular activity rate, z is the z-score, BS is the baseline cellular activity rate and k is the scaling factor. k scales the effect of the z-score and is calculated using the following line slope equation:

$$k = \frac{Y_2 - Y_1}{z_2 - z_1} = \frac{(BS \times 2) - BS}{2 - 0} = \frac{BS}{2} \tag{2}$$

To establish a linear relationship between the z-score and the cellular activity rate when calculating the scaling factor k, it was assumed that when the z-score is 0, showing neither inhibition nor activation, the cellular activity rate (Y) stays at its baseline level ($Y_1 = \mathrm{BS}$). On the other hand, when the z-score is 2, indicating activation, the cellular activity rate doubles from its baseline value, representing a 100 % impact of the z-score on the cellular activity rate ($Y_2 = \mathrm{BS} \times 2$). Using these equations, a specific z-score of a biological process would impact all activities similarly.

In general, cell activities rates in the ABM indicate the % of cells performing the specific activity per each iteration (i.e. per day). Therefore, activity rates range from 0 to 100 %, excluding cell migration rate which is given in μm/day. Additionally, if protein expression changes are given at multiple time points during the healing process, the unmeasured protein expressions between two time points are obtained using linear interpolation.

In the final step, the simulations are carried out, yielding personalized healing outcomes based on their distinctive proteomic expressions (Fig. 1).

Table 1
Biological processes in ABM and their counter biological processes in IPA.

Biological processes	
ABM parameter	IPA (z-score)
MSC migration rate	Migration of cells
Fibroblast migration rate	Migration of fibroblasts
Fibroblast differentiation rate	Differentiation of connective tissue cells
Chondrocyte differentiation rate	Differentiation of connective tissue cells
Osteoblast differentiation rate	Differentiation of osteoblasts
MSC proliferation rate	Proliferation of progenitor cells
Fibroblast proliferation rate	Cell proliferation of fibroblasts
Chondrocyte proliferation rate	Proliferation of connective tissue cells
Osteoblast proliferation rate	Proliferation of connective tissue cells
Fibroblast apoptosis rate	Apoptosis of connective tissue cells
Chondrocyte apoptosis rate	Apoptosis of connective tissue cells
Osteoblast apoptosis rate	Apoptosis of connective tissue cells

2.3. Evaluation of the OMIBONE framework

The OMIBONE framework was evaluated for its potential to predict the bone healing outcome in a mouse femur fracture model stabilized with an intramedullary nail [27].

2.3.1. Description of the simulated experiment

Briefly, in a previous study, a targeted proteomic analysis of mouse serum was carried out to monitor the biological progression of fracture healing over a 35-day period [27]. Transverse, closed femoral fractures were generated and stabilized with intramedullary fixation in male C57BL/6J (B6) mice (Jackson Laboratories, Bar Harbor, ME), 8–12 weeks of age ($n = 6$ per time point). A single stranded DNA aptamer-based multiplexed proteomic approach was used to assay 1310 proteins. Samples from unfractured femoral bones from male mice of the same starting age as those that had been fractured were used as the reference (day 0). Proteomics data were collected at multiple points (0, 3, 7, 10, 14, 21 and 35 days post-fracture), where the fold change of the proteomics was taken relative to day 0 (non-fractured). Of the 1310 proteins analysed, 850 proteins showed significant differences among the time points (p-value < 0.05) (Supplementary material).

X–ray images of the fracture callus as well as transverse histological sections in the middle of the fracture calluses were performed at different time points post-fracture to monitor the biological progression

of fracture healing. Additionally, RT-PCR was carried out on selected genes for validation [82], where the RT-PCR mRNA expression levels of markers associated with cartilage (Aggrecan) and bone (Osteocalcin) differentiation were quantified.

2.3.2. Finite element model of the experimental setup

To replicate the experimental setup [27], an FE model was created to assess the mechanical environment inside the fracture. The FE model was developed in ABAQUS/Standard 2019 (Simulia, Dassault Systèmes). The model simulated a fracture in the mouse femur stabilized with an intramedullary nail [27]. The computer model included the cortical bone, the marrow cavity, and the intramedullary nail surrounded by a callus (Fig. 2). All geometry dimensions are based on the experimental data and are provided in Supplementary material [39,40].

The model was meshed using three-dimensional quadratic tetrahedral elements with an average mesh size of 0.50 mm for the whole model except for the callus region, where the average mesh size was 0.10 mm. This resulted in a total number of 232,682 nodes and 163,033 elements.

All biological tissues were modeled as poroelastic materials with properties given in Table 2. The intramedullary nail was made of stainless steel [41]. Linear elastic isotropic properties were assigned to the nail (E = 190 GPa, v = 0.3).

The loading conditions applied are intended to simulate the mechanical environment experienced by the bone during gait. Compression and bending loads were applied as previously reported [39]. The FE model assumed an average mouse body weight of 0.025 kg [39,40]. A 1.8 N compression load was applied at the proximal bone end to achieve a 6 BW in compression [42]. Two tangential concentrated forces of 0.35 N were applied at the proximal bone end in the medial/lateral and anterior/posterior directions to achieve a 10.7 BW mm (2.6 Nmm) bending moment at the femoral mid-shaft [42]. Boundary conditions were applied on the other bone end (distal end) to restrain the movement in all directions. The predicted compressive minimum principal strains of the mouse fractured femur FE model are shown in both the longitudinal and transverse mid-sections of the callus in Fig. 2.

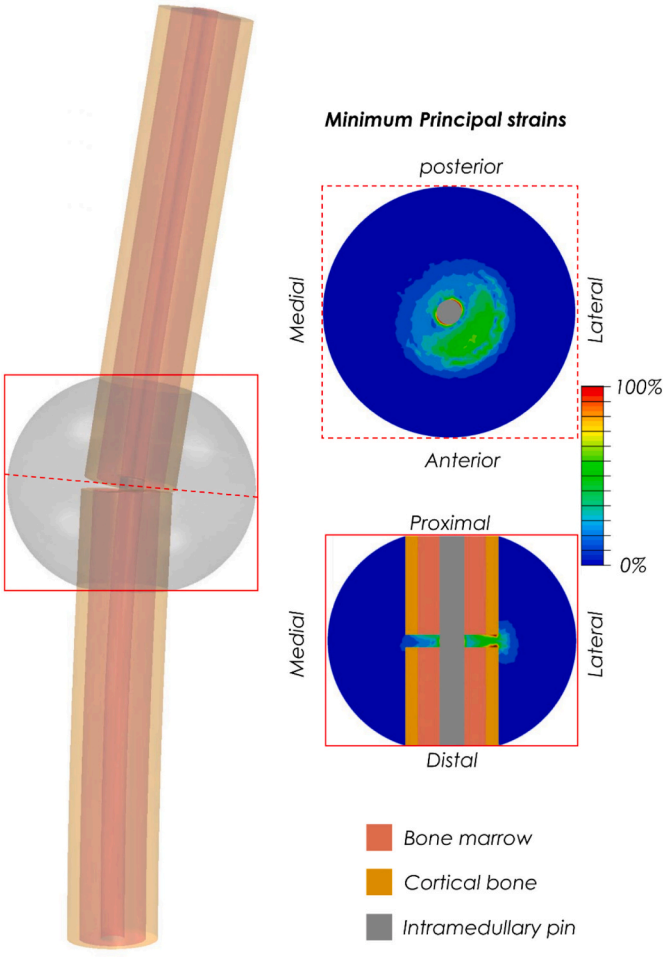

Fig. 2. Deformed finite element model of the mouse femoral fracture stabilized with an intramedullary nail (following the experimental setup of [27]). Predicted compressive minimum principal strains in both longitudinal and transverse mid-sections of the callus are shown in solid and dashed borderlines, respectively.

2.3.3. Omics-based prediction of bone regeneration

OMIBONE was tested in two different situations: 1) OMIBONE (Exp.): a healing situation which aim to replicate the experiment described in [27] and 2) OMIBONE (Mod.): a non-healing situation which was virtually created by modifying the proteomics data reported in Hussein et al.

As described in the previous Section 2.3, a downstream effects analysis was conducted on the proteomics data from the experiment [27], assigning a z-score to each biological process as outlined in Table 2. These z-scores were calculated for each biological process at various time points (3, 7, 10, 14, 21, and 35 days), providing insights into the activation and inhibition of these processes during the healing process.

In addition, to test OMIBONE's predictive capacity in non-healthy conditions, the proteomics data from Hussein et al. [27] was modified (Supplementary material). This modification involved altering the up and downregulation directions of a subset of proteins, specifically 22 out of 852 proteins (Supplementary material). The modification was done by changing only the direction of regulation; i.e. up regulated proteins become down regulated and vice versa, while keeping the magnitude of protein expression unchanged. Selected proteins were based on previous studies showing a detrimental effect of the specific protein on cellular function. Table 3 shows the selected proteins and their associated biological function. During the selection process, priority was given to proteins involved in multiple biological processes and those with a higher z-score; i.e. higher impact on biological activity, as determined by IPA.

The z-score of the biological processes at several time points of both, the experimental proteomics [27] and the modified ones (non-healthy condition), are given in Fig. 3.

Applying Eq. (1) to the z-scores of the biological processes, the mapped cellular activities rates become time dependent, in contrast to the constant values used in the baseline model. The time dependent mapped cellular activities rates serving as input to the ABM are given in Fig. 4.

To evaluate the effect of varying scaling factors on the bone healing predictions outcome, a parametric analysis was performed. OMIBONE was run with scaling factor *k*: *BS/4*, *BS/16*, *BS*, *BS x 2* and *BS x 4*.

2.4. Output analysis

The bone healing process within the mouse femur fracture stabilized with an intramedullary nail, following the experimental set up of Hussein et al., was simulated using the OMIBONE framework using both OMIBONE (Exp.): based on proteomics from the experiment [27] and OMIBONE (Mod.): based on modified proteomics (representing a non-healthy situation) as input parameters.

2.4.1. X-ray-like images and bone volume to total volume (BV/TV %)

To compare the time evolution of the bone healing process within the fracture with experimental data, X-ray-like images were computationally generated at the same time points than in the experiment [27], i.e. at 7, 21, and 35 days post-surgery; using the algorithm from Perier-Metz et al. [35]. The algorithm uses the Beer-Lambert law, which models how

Table 2
Tissue material properties (adapted from [32]).

	Granulation tissue	Fibrous tissue	Cartilage	Immature bone	Mature bone	Cortical bone	Bone marrow
Young's modulus (MPa)	0.2	2	10	1000	5000	5000	2
Permeability (10^{-14} s.m^4/N)	1	1	0.5	10	37	0.001	1
Poisson's ratio	0.167	0.167	0.3	0.3	0.3	0.3	0.167
Bulk modulus grain (MPa)	2300	2300	3700	13,940	13,940	13,920	2300
Bulk modulus fluid (MPa)	2300	2300	2300	2300	2300	3200	2300

Table 3
Selected proteins for which their regulation direction was altered in relation to the experimental proteomics by Hussein et al. [27]. Full data of the modified proteomics are available as an excel sheet in the Supplementary material.

Protein	Related biological process
TP53	Apoptosis of connective tissue cells, proliferation of progenitor cells, cell proliferation to fibroblasts, differentiation of osteoblasts, migration of fibroblasts, proliferation of connective tissue cells, and migration of cells.
FASLG	Apoptosis of connective tissue cells and differentiation of osteoblasts.
BCL2	Apoptosis of connective tissue cells, differentiation of osteoblasts, and migration of cells.
AGT	Apoptosis of connective tissue cells, cell proliferation to fibroblasts, migration of fibroblasts, proliferation of connective tissue cells, and migration of cells.
IGF1	Apoptosis of connective tissue cells, proliferation of progenitor cells, cell proliferation to fibroblasts, differentiation of connective tissue cells, differentiation of osteoblasts, migration of connective tissue cells, proliferation of connective tissue cells, and migration of cells.
RAC1	Apoptosis of connective tissue cells, cell proliferation to fibroblasts, migration of fibroblasts, and migration of cells.
VEGFA	Apoptosis of connective tissue cells, proliferation of progenitor cells, differentiation of connective tissue cells, differentiation of osteoblasts, and migration of cells.
IL4	Apoptosis of connective tissue cells, proliferation of progenitor cells, cell proliferation to fibroblasts, differentiation of connective tissue cells, migration of connective tissue cells, proliferation of connective tissue cells, and migration of cells.
JAK2	Proliferation of progenitor cells and migration of cells.
SHH	Proliferation of progenitor cells, differentiation of connective tissue cells, and differentiation of osteoblasts.
THPO	Proliferation of progenitor cells.
CSF3	Proliferation of progenitor cells.
MSTN	Proliferation of progenitor cells, cell proliferation to fibroblasts, differentiation of connective tissue cells, differentiation of osteoblasts, and proliferation of connective tissue cells.
BMP6	Proliferation of progenitor cells, differentiation of connective tissue cells, and differentiation of osteoblasts.
CXCL12	Cell proliferation to fibroblasts, migration of fibroblasts, proliferation of connective tissue cells, and migration of cells.
F2	Cell proliferation to fibroblasts, proliferation of connective tissue cells, and migration of cells.
BMP7	Differentiation of connective tissue cells and differentiation of osteoblasts.
GDF11	Differentiation of connective tissue cells and differentiation of osteoblasts.
PTH	Apoptosis of connective tissue cells, differentiation of connective tissue cells, and differentiation of osteoblasts.
SERPINF1	Differentiation of osteoblasts and migration of fibroblasts.
EGF	Apoptosis to connective tissue cells, proliferation of progenitor cells, cell proliferation to fibroblasts, migration of fibroblasts, proliferation of connective tissue cells, and migration of cells.
CSF2	Proliferation of progenitor cells.

X-ray intensity decreases through a material and ignores the surrounding soft tissues and their X-ray scattering [35]. The images are generated based on material/sample thickness and attenuation data [35].

In addition, the bone volume to total volume (BV/TV %) in the healing region was obtained by quantifying the total amount of bone formed per day relative to the total volume of the callus (25 mm^3) at the same time points than in the experiment [27], i.e. at 14, 21, and 35 days post-surgery.

2.4.2. Histological-like images

Transverse histological-like sections at the middle of the fracture callus at 14- and 21-days post-fracture were generated to monitor the progression of predicted cartilage and bone tissue formation, similar to the experiment [27]. The computer model images used colors similar to the experiment's images of Safranin O/Fast Green Stain staining [27], with bone shown in blue and cartilage in red, while empty areas and the intermedullary pin were depicted in white.

2.4.3. Cellular activities output

To compare the experimental temporal dynamics of QR-mRNA expression of osteoblast and chondrocyte differentiation markers, given by Osteocalcin and Aggrecan, respectively [27], cellular activities in the computer model were quantified. Predicted chondrocyte and osteoblast differentiation within the callus were quantified by measuring the total number of MSCs differentiated into chondrocytes and osteoblasts daily until day 35, relative to the total volume of the callus.

3. Results

3.1. Mechanical strains within the callus in a pinned mouse fracture model

The compressive minimum principal strains varied across the callus and showed an asymmetric distribution due to asymmetric loading conditions (Fig. 2). In general, higher strains were predicted at the intercortical and endosteal regions than in the periosteal region. The maximum levels of strains were predicted in the lateral anterior direction. Quantitatively, in the medial side, the FE model predicted strains in the range of 35 %–72 %, 15 %–45 % and 10 %–40 % in the intercortical, endosteal and periosteal regions, respectively. In the lateral side, lower strains were predicted compared to the medial side with values of 4 %–20 %, 15 %–45 % and 0 %–10 % in the intercortical, endosteal and periosteal regions, respectively.

3.2. Proteomics-driven OMIBONE is able to capture the progression of bone regeneration

At the early phase of healing (day 7), a clear fracture line was observed both experimentally and in the predictions by the computer model (Fig. 5A). By day 21, complete callus bridging was already observed both in experiment and in OMIBONE (Exp.); with OMIBONE (Exp.) predictions showing a lower bone formation response. By day 35, bone formation with the OMIBONE model showed bone bridging and callus formation similar to the one observed experimentally; however, with a larger callus being predicted by OMIBONE (Exp.) (Fig. 5A). Furthermore, due to asymmetrical mechanical strain distributions in the callus (Fig. 1), a slight asymmetry in bone distribution was predicted (Fig. 5A).

Quantitative analysis of the bone healing outcome showed higher differences in terms of BV/TV between simulation predictions and experimental data (Fig. 5B). At day 14, higher bone formation was observed within fracture gap experimentally (BV/TV: 8.2 % ± 1.86 %) than with OMIBONE (Exp.) (BV/TV: 0.87 %). At day 21, BV/TV was 16.2 % ± 3.72 % and 9 % in the experiment and OMIBONE (Exp.),

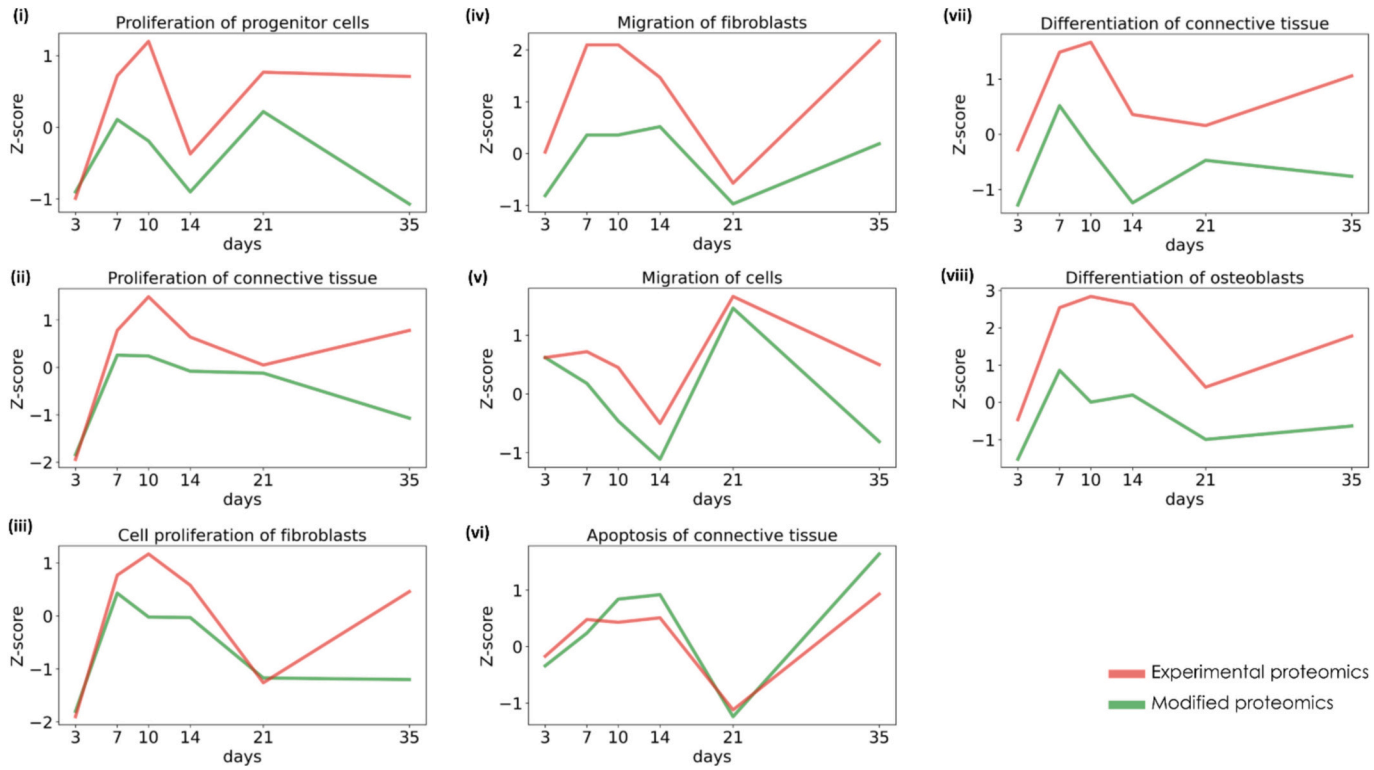

Fig. 3. z-Score values derived from the IPA software for the proteomics data from Hussein et al. [27] and those modified to simulated a non-healthy condition.

respectively. At the end of the healing, on day 35, the computer model predicted higher bone formation as the one reported experimentally (OMIBONE (Exp.)): 39 %, experiment 19.6 % ± 2.56 %.

3.3. OMIBONE reproduces experimentally observed endochondral ossification

Fig. 6 presents the cartilage and bone tissue formation patterns in a transverse cross-section through the callus, observed experimentally and predicted using the OMIBONE (Exp.) model. At day 14, cartilage formation was observed both experimentally and with the OMIBONE (Exp.) computer model. However, a higher proportion of bone tissue was observed in the experimental case compared to the simulation. By day 21, cartilage had undergone complete replacement by bone tissue experimentally with signs of bone resorption (Fig. 6). Similarly, computer model predictions showed cartilage replacement by bone tissue. Notably, the asymmetric cartilage formation in the callus followed the asymmetric mechanical strains (Fig. 1), where regions with higher mechanical strains lead to cartilage formation and regions with lower mechanical strains lead to bone formation (Fig. 6).

3.4. Bone healing biomarkers confirm OMIBONE cellular behaviour progression

On day 3, cartilage formation, as indicated experimentally by Aggrecan expression, was observed at a low level. By day 7, a substantial increase was observed until day 10, before undergoing a strong decline by day 14 and continuing in this trend until the end of the regeneration process at day 35 (Fig. 7A). OMIBONE (Exp.) predictions exhibited a similar pattern in terms of chondrocyte differentiation, beginning with low values on day 3, followed by a steady rise until around day 7. Thereafter, OMIBONE (Exp.) chondrocyte differentiation reached its peak between day 11 and 13, followed by a sharp decline by day 15, and continuing in this trend until the end of the regeneration process at day 35 (Fig. 7B).

A similar temporal pattern was also observed between the bone formation marker Osteocalcin and the OMIBONE (Exp.) predicted osteoblast differentiation. Experimentally, an initial low expression of the bone formation marker Osteocalcin was observed between days 3 and 7. By day 7, a slight increase was observed, followed by a gradual increase on days 10 and 14, reaching its highest observed expression level by day 21. Thereafter, a decline was observed until day 35 (Fig. 7A). OMIBONE (Exp.) predictions were similar in terms of osteoblast differentiation (Fig. 7B). Around day 30, OMIBONE predicted the peak of osteoblast differentiation, followed by a decline until the end of the regeneration (Fig. 7B).

3.5. OMIBONE predicted altered healing using modified proteomics

Using modified proteomics as an input to OMIBONE led to an altered bone healing prediction when compared to the experimental data. A slower bone healing response was predicted using the modified proteomics data in addition to a reduced bone and cartilage tissue formation response, evident both histologically and in terms of predicted cellular activity dynamics (Fig. 8).

3.6. OMIBONE's sensitivity to varying scaling factor

The parametric analysis revealed the effect of the scaling factor on the healing outcome predictions. In general, changes in the scaling factor did not alter the bone healing prediction dynamics. For all scaling factors, an increase of BV/TV was predicted from day 14 to 36, as reported experimentally. At day 14, all models with different scaling factors resulted in low BV/TV values (around 1 %). At day 21, variations in scaling factors between BS/16 and BSx4 resulted in differences in predicted BV/TV of around 5 %. The highest BV/TV was predicted for a scaling factor of BS/2. Increasing or decreasing the scaling factor led to a decrease in the predicted BV/TV (Fig. 9).

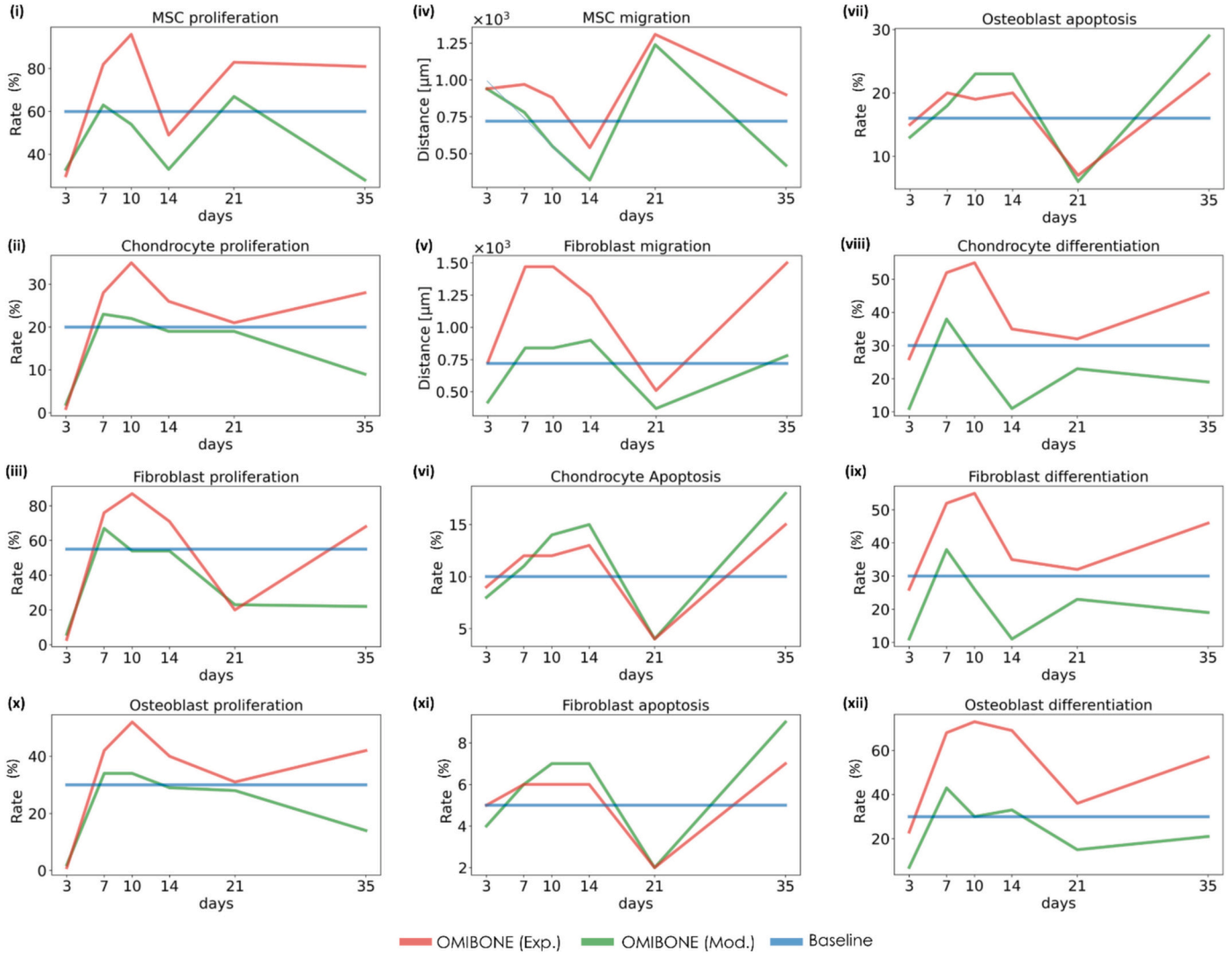

Fig. 4. Cellular activities rates at multiple time points (days: 3, 7, 10, 14, 21 and 35) OMIBONE (Exp.): based on the experiment from Hussein et al. [27]; OMIBONE (Mod): based on modified protein changes to represent a non-healthy situation; Baseline: rates of the baseline bone healing model adapted from Checa et al. [32].

4. Discussion

In the last years, the development of personalized patient-specific computer models of bone regeneration, where it becomes possible to tailor predictions to each patient's specific intrinsic regenerative capacity, has gained considerable attention [43,44]. However, a computer model that considers the patient's unique healing potential is not available. In this study, a previously validated computer model of bone regeneration [32] was further developed to include the patient's regeneration potential by incorporating proteomics data; yielding OMIBONE. The framework combined proteomic and mechanical analyses in computational modeling to facilitate predictions of bone regeneration outcomes. In this framework, IPA software was utilized to link the impact of protein regulations on cellular function. OMIBONE successfully captured the progression of bone regeneration in a mouse fracture stabilized with an intramedullary pin, including the experimentally observed endochondral ossification process.

In this study, we coupled omics data with an ABM of bone regeneration. Recently, only a few studies have linked agent-based models to omics data [45–48]. Different approaches have been used such as using mathematical equations, Boolean approaches, and specifically designed algorithms to study cancer, drug effects on cancer and in-stent restenosis, respectively [45,46,48]. Further, Retzlaff et al. used omics to select impactful cancer-related biological processes in their cancer model, thereby reducing model's parameters [47]. Although all models were able to predict to some extent the expected cellular behaviour, computer model predictions were never compared to experimental data. In this study, OMIBONE employed the z-score of the software IPA to guide cellular activities involved in bone regeneration and predicted outcome was compared to experimental data. IPA Downstream Effects analysis was applied to predict the biological processes regulated by proteins with changed expression levels, attributing a z-score to each process. It was assumed that the probability of activation or inhibition, as indicated by the z-score, is proportional to the rate of the biological function. This enabled the estimation of the cellular activity rates that were incorporated into the ABM. This approach associates proteomics data to functional cellular activity rates; however, the z-scores being proportional to activity rates remains an assumption and should be further investigated in the future.

Previously, IPA's z-score has been used in a number of studies related to bone tissue. For instance, IPA's z-score was used to reveal key processes in in vivo bone regeneration studies, including Type 2 Diabetes [49], implant properties [50], spinal cord changes after fractures [51], periodontal tissue profiles [52], and metabolic patterns in femur head necrosis [53]. In addition, several in vitro studies used IPA's z-score to identify activation/inhibition of biological processes related to bone regeneration such as chondrogenesis [54], osteogenesis [55,56], adipogenesis [57], inflammation modulation [58], and tissue healing [59].

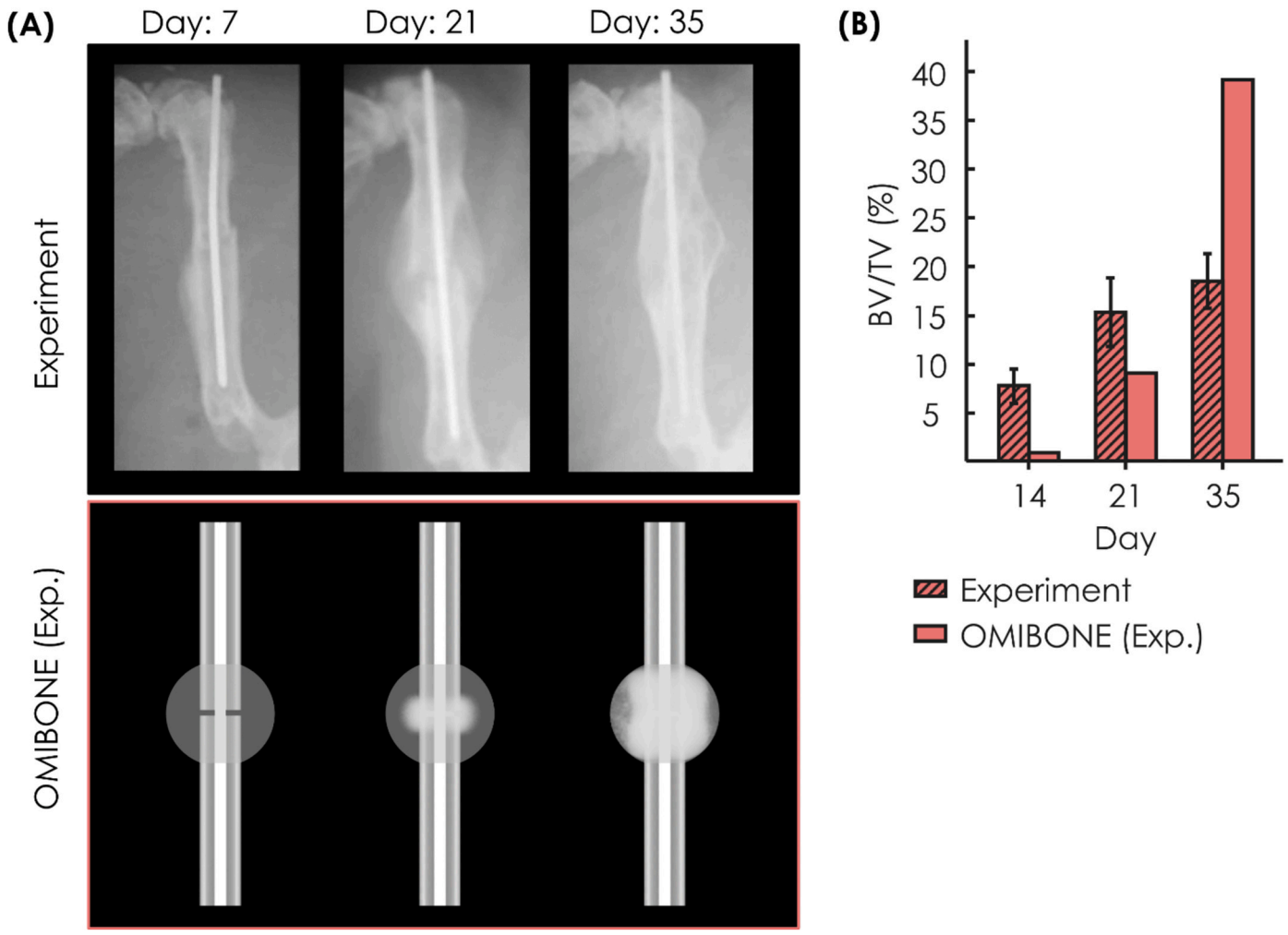

Fig. 5. (A) Representative x-ray images from the experiment [27] as well as from the simulations in OMIBONE (Exp.). (B) Comparison of predicted BV/TV % to the experimental data from SIMMONS, 2013.

In this study, IPA's z-score revealed the temporal dynamics of biological processes involved in fracture healing experiments in mouse [27]. Interestingly, the temporal variation of the cellular maker, e.g. Osteocalcin, showed a temporal delay with respect to the z-score associated with a specific cellular process, e.g. osteoblast differentiation. Both, osteoblast and chondrocyte differentiation showed a temporal delay relative to Osteocalcin and Aggrecan expressions. These differences can be explained by the interaction of the many cellular processes taking place during bone regeneration.

In this study, OMIBONE adapted an FE model with a simplified osteotomy geometry, following the geometry and material properties of a previously validated bone regeneration model in mice [31]. The compressive mechanical strains predicted within this study compared well to those from previous studies [31]. Numerous computer models of bone regeneration have in the past adopted similar simplified computational strategies [32,35,38,60–66]. These models have proven effective in simulating major biological phases of bone healing [32,38,61–63], identifying key factors that impair bone regeneration under compromised conditions [31,33], and investigating the impact of implants on the bone healing outcome [34,35,60].

The predictive healing capacity of OMIBONE was assessed by comparing the prediction of healing progression to an existing experiment of fracture healing in a mouse femur stabilized with an intramedullary pin [27]. When proteomics from the experiment [27] were used as an input in OMIBONE, the model was able to capture the progression of bone regeneration, as observed in X-ray images. In addition, OMIBONE reproduced experimentally observed endochondral ossification where initially cartilage formation was observed, followed by replacement by bone tissue. Moreover, the higher amount of cartilage tissue predicted on one side of the fracture callus is in agreement with histological observations [27,67,68]. OMIBONE's predictive healing ability was further validated by comparing experimentally measured bone healing biomarkers (Osteocalcin and Aggrecan) with temporal changes in cellular behaviour (MSC differentiation into chondrocytes and osteoblasts) predicted with OMIBONE. Predicted osteoblast and chondrocyte differentiation by OMIBONE compared well with the temporal dynamics of QR-mRNA expression of bone and cartilage differentiation markers, given by Osteocalcin and Aggrecan, respectively.

OMIBONE is based on a previously validated bone regeneration computer model that relies on constant parameters to describe the rates of the different cellular activities during the regeneration process [31,32]. The model has been previously used to predict bone regeneration in different pre-clinical studies under different conditions [31–33]. To further test the prediction potential of the baseline model and the influence of the omics-based computer model developed in this study, the experiment by Hussein et al. [27] was also simulated with the baseline model by Checa et al. [32]. Model predictions were close to those reported experimentally and those predicted by the OMIBONE model but with less bone predicted with the baseline model (Supplementary material). In addition, OMIBONE was tested by using modified omics data as input to the same simulated experimental setting, representing a non-healthy situation. The expression of proteins that promote

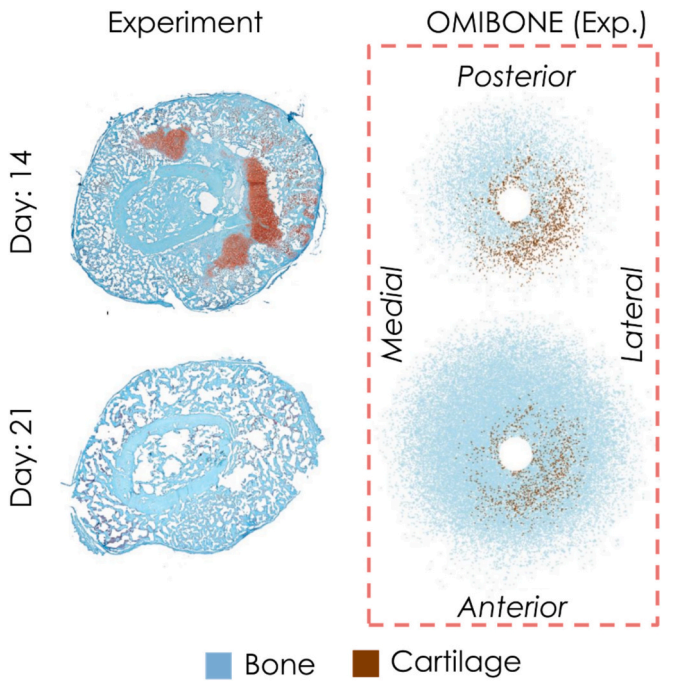

Fig. 6. Biological progression of fracture healing from the experiment [27] as well as from the simulations in OMIBONE (Exp.): based on the experiment from Hussein et al. [27]. Histological sections of fracture calluses at: 14- and 21-days post-fracture. Cartilage stains red with safranin O and bone stains greenish blue with fast green from the experiment [27]. (For interpretation of the references to color in this figure legend, the reader is referred to the web version of this article.)

key activities like osteoblast differentiation and MSC proliferation were decreased, while proteins involved in degenerative processes like apoptosis were increased. Clinically, this reflects conditions including cancer, osteoporosis, autoimmune disorders, diabetes and cardiovascular diseases [69–73], where bone regeneration is compromised. For example, IGF1, crucial for several key cell activities, is linked to osteoporosis [71], and VEGFA, essential for angiogenesis [74], is associated with diabetes [73]. In this case, reduced and slower tissue formation was predicted in both virtual X-ray and histological images compared with those from the experimental setup. Additionally, reduced osteoblast and chondrocyte differentiation levels were predicted. These findings reflect OMIBONE's sensitivity to proteomics data.

This study has several limitations. The BV/TV predicted by OMIBONE did not quantitatively match the one observed experimentally. At the initial healing phases, lower bone formation was predicted compared with the experimental data. At day 21, more bone was already observed within the experiment compared to OMIBONE. However, at the end of the healing period, the model predicted higher bone formation compared with the experimental data. One reason of these differences could be due to the baseline rates of the cellular activities used in OMIBONE. Previous studies using the computer model of bone regeneration used here also reported a slower predicted bone formation response in comparison to the experiment [39]. They suggested that the slower healing observed in the model was due to the fact that the cellular activity rates used in their computer model were based on rats, where healing is usually slower than in mice [39]. In this study, cellular activity rates were scaled according to the IPA's z-score following a linear relation, with a scale factor of BS/2; where BS refers to the rates used in Checa et al. [32]. In a parametric analysis, we investigated the effect of the scaling factor on the healing predictions. Since this factor acts on the z-score, it influences both the activation and inhibition of cellular activities over the healing process. For instance, a high scaling factor results in an increase in the cellular activity rate if the corresponding biological process was activated (positive z-score) at a certain time point; however, it also results in a decrease in the cellular activity rate if

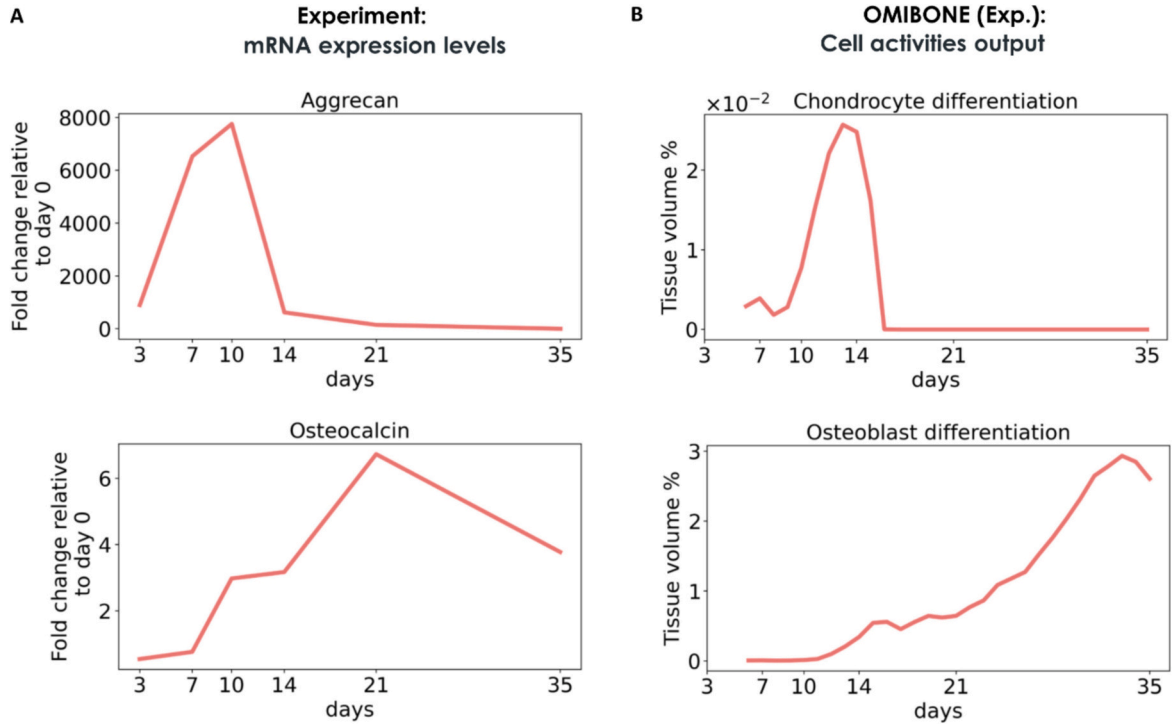

Fig. 7. (A) quantitative RT-PCR mRNA expression levels of markers of chondrocyte (Aggrecan) and osteoblast (Osteocalcin) differentiation relative to day 0 (non-fractured bone; adapted from Hussein et al. [27]). (B): Differentiation of chondrocytes and osteoblasts in terms of volume over total volume as predicted by OMIBONE (Exp.). Total volume of callus = 25 mm^3.

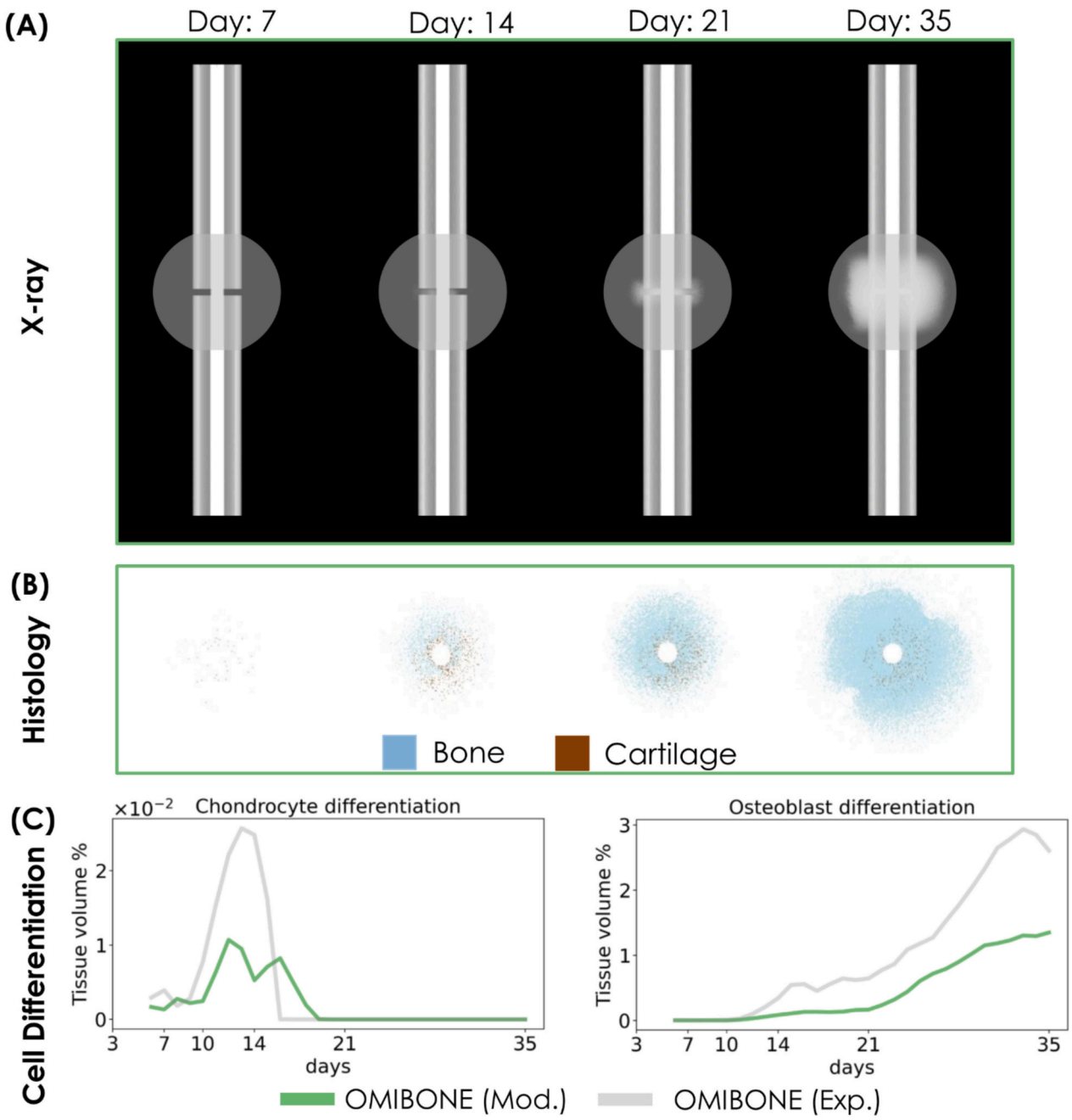

Fig. 8. (A) X-ray-like images, (B) Histological-like images, and (C) Cell differentiation of osteoblasts and chondrocytes throughout the regeneration as predicted by OMIBONE (Mod.): based on modified protein changes to represent a non-healthy situation.

the corresponding biological process was inhibited (negative z-score) (Supplementary material). Therefore, a high scaling factor would not necessarily lead to an increase in cellular activity rates, which can explain why low and high scaling factors result in reduced predicted bone healing outcome. Future studies are needed to further investigate the relation between proteomics signals and cellular function in the context of bone regeneration.

Furthermore, the OMIBONE framework was tested on a single experimental setup involving healthy controlled animals and their proteomics data. To our knowledge, the experimental study by Hussein et al. [27] is the only one reporting longitudinal plasma proteomics data during a bone regeneration process. In a first attempt to test the OMIBONE framework on predicting patient-specific healing outcome, the proteomics data by Hussein et al. [27] were modified. While the model was able to predict different healing outcome based on different proteomics levels, there is a need to validate those results. The validation of OMIBONE in different experimental setups which could also include compromised conditions, such as T2DM or osteoporosis, remains to be performed. In addition, experiments could be performed in parallel to simulations, ensuring experimental conditions are well replicated and allowing for real-time validation. Finally, in the current application of OMIBONE, proteomics data at multiple time points during the healing process was used, which would not be possible in a human context. Future work should focus on using OMIBONE as a prognosis tool whereby healing outcome can be predicted based on proteomics data derived from pre or post-surgery situations.

With the aim to validate the biomechanical behaviour of the finite element model, we performed a virtual torsional testing of the intact and fractured bones and compared the predicted values to the experimental literature. The predicted torsional stiffness was 47 Nmm/rad for the

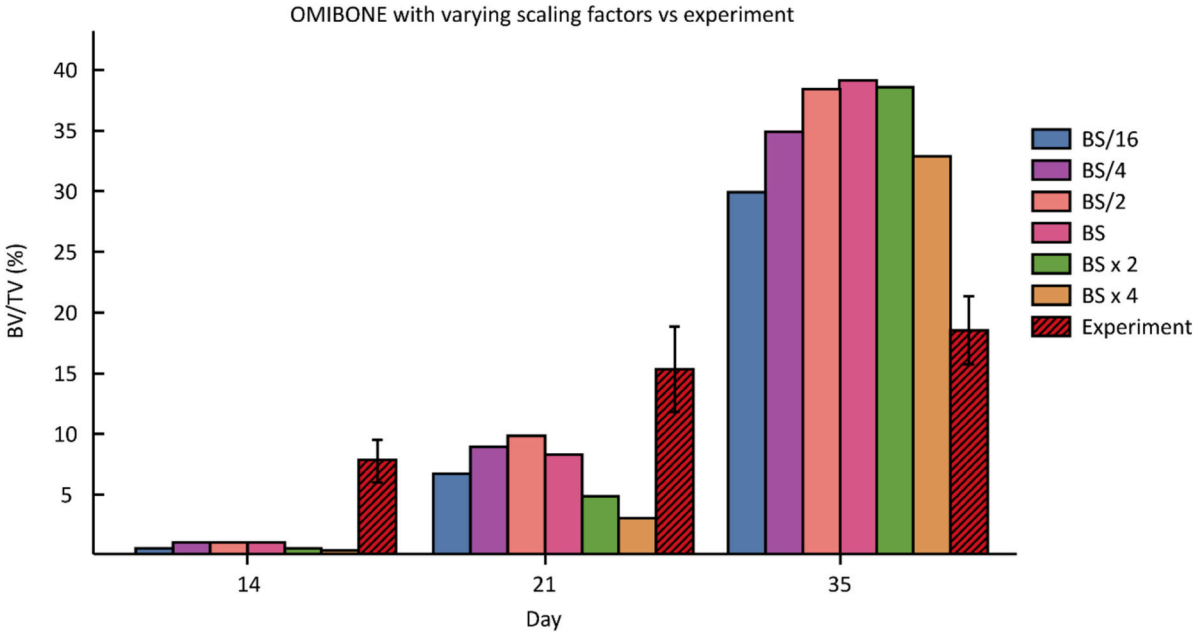

Fig. 9. Bone volume to total volume, BV/TV (%) of OMIBONE with varying scaling factors, k = BS/2, BS/4, BS/16, BS and BS x 4 and experiment data [27]. Total volume of callus = 25 mm^3.

intact bone and 59 Nmm/rad for the fractured bone at day 21 post-fracture. Experimentally, using the same animal model, Simmon, 2013, reported a rotational stiffness of 410 Nmm/rad in intact femur and 278 Nmm/rad and 410 Nmm/rad post-fracture, at days 14 and 21, respectively [75]. However, Jepsen et al. [68] reported a stiffness in intact bone of 6.4 Nmm/rad [68]. Post fracture at days 21 and 35, they reported 5.8 Nmm/rad and 7.4 Nmm/rad, respectively [68]. O'Neill et al. [76] with similar experimental setup and mouse strain but different sex, reported a stiffness for intact bone of 1.08 Nmm/rad and post fracture, at days 14, 21 and 35 of 0.91 Nmm/rad, 0.97 Nmm/rad and 0.86 Nmm/rad, respectively [76]. Pelch et al. [77] reported 79.46 Nmm/rad and Camacho et al. [78] reported 3.66 Nmm/rad in the intact bone for the same mouse strain and sex [77,78]. Kruck et al. reported a torsional stiffness of 229 Nmm/rad for the intact femur of the same mice but different sex [79]. Finally, Holstein et al. [80] reported a torsional stiffness of 95 Nmm/rad in the intact femur of mice of the same strain [80]. Although, the predicted values fall within those reported experimentally, the broad range of experimental values makes the validation of the model challenging. Future studies are needed where experimental and numerical analyses are combined to investigate the biomechanics of fractured bone. One possible reason behind the variability of the experimental data could be the gauge length (the portion of the bone left exposed for testing), which is not reported in the majority of the studies. In this study, we conducted additional FE simulations using a 6 mm gauge length [81], leading to torsional stiffness of 115 Nmm/rad.

In summary, we developed a computational framework of bone regeneration namely, OMIBONE, that combined mechanical analyses and proteomics data to predict an individual-specific healing outcome. OMIBONE was able to predict similar bone healing progression as observed experimentally in a mouse fracture model. In addition, OMIBONE was able to predict altered bone regeneration based on modified proteomics profiles. OMIBONE holds promise as a tool for clinicians to predict bone healing and inform personalized treatment strategies.

CRediT authorship contribution statement

Mahdi Jaber: Writing – review & editing, Writing – original draft, Visualization, Validation, Software, Methodology, Investigation, Formal analysis, Data curation, Conceptualization. **Johannes Schmidt:** Writing – review & editing, Validation, Formal analysis. **Stefan Kalkhof:** Writing – review & editing, Validation, Formal analysis, Data curation. **Louis Gerstenfeld:** Writing – review & editing, Validation, Resources, Methodology, Investigation, Formal analysis. **Georg N. Duda:** Writing – review & editing, Validation, Supervision, Resources, Project administration, Formal analysis. **Sara Checa:** Writing – review & editing, Writing – original draft, Validation, Supervision, Resources, Project administration, Investigation, Funding acquisition, Formal analysis, Conceptualization.

Declaration of competing interest

The authors have no conflicts of interest to declare. All co-authors have seen and agree with the contents of the manuscript and there is no financial interest to report. We certify that the submission is original work and is not under review at any other publication.

Acknowledgments

This study was funded by the BMBF, SyMBoD project 01ZX 1910A.

Appendix A. Supplementary data

Supplementary data to this article can be found online at https://doi.org/10.1016/j.bone.2024.117288.

Data availability

The authors confirm that the data supporting the findings of this study are available within the article and its Supplementary materials. Any further data that support the findings of this study are available from the corresponding author upon reasonable request.

References

[1] Donald A. Wiss, W.B. Stetson, Tibial nonunion: treatment alternatives, J. Am. Acad. Orthop. Surg. 4 (1996) 249–257.
[2] C. Arrigoni, M. Gilardi, S. Bersini, C. Candrian, M. Moretti, Bioprinting and organ-on-chip applications towards personalized medicine for bone diseases, Stem Cell

Rev. Rep. 13 (2017) 407–417, https://doi.org/10.1007/S12015-017-9741-5/FIGURES/2.
[3] E.R. Pearson, Personalized medicine in diabetes: the role of 'omics' and biomarkers, Diabet. Med. 33 (2016) 712–717, https://doi.org/10.1111/DME.13075.
[4] R. Chen, M. Snyder, Promise of personalized omics to precision medicine, Wiley Interdiscip. Rev. Syst. Biol. Med. 5 (2013) 73–82, https://doi.org/10.1002/WSBM.1198.
[5] L.H. Goetz, N.J. Schork, Personalized medicine: motivation, challenges, and progress, Fertil. Steril. 109 (2018) 952–963, https://doi.org/10.1016/J.FERTNSTERT.2018.05.006.
[6] M. Mann, O.N. Jensen, Proteomic analysis of post-translational modifications, Nat. Biotechnol. 213 (21) (2003) 255–261, https://doi.org/10.1038/nbt0303-255.
[7] D. Lendeckel, C. Eymann, P. Emicke, G. Daeschlein, K. Darm, S. O'Neil, et al., Proteomic changes of tissue-tolerable plasma treated airway epithelial cells and their relation to wound healing, Biomed. Res. Int. 2015 (2015), https://doi.org/10.1155/2015/506059.
[8] M. Li, Z.Q. Xiao, Z.C. Chen, J.N. Li, C. Li, P.F. Zhang, et al., Proteomic analysis of the aging-related proteins in human normal colon epithelial tissue, J. Biochem. Mol. Biol. 40 (2007) 72–81, https://doi.org/10.5483/bmbrep.2007.40.1.072.
[9] J.R. Peters-Hall, K.J. Brown, D.K. Pillai, A. Tomney, L.M. Garvin, X. Wu, et al., Quantitative proteomics reveals an altered cystic fibrosis in vitro bronchial epithelial secretome, Am. J. Respir. Cell Mol. Biol. 53 (2015) 22–32, https://doi.org/10.1165/RCMB.2014-0256RC/SUPPL_FILE/DISCLOSURES.PDF.
[10] H.C.A. Drexler, A. Ruhs, A. Konzer, L. Mendler, M. Bruckskotten, M. Loosos, et al., On marathons and sprints: an integrated quantitative proteomics and transcriptomics analysis of differences between slow and fast muscle fibers, Mol. Cell. Proteomics 11 (2012), https://doi.org/10.1074/mcp.M111.010801.
[11] B.W. Kong, K. Lassiter, A. Piekarski-Welsher, S. Dridi, A. Reverter-Gomez, N. J. Hudson, et al., Proteomics of breast muscle tissue associated with the phenotypic expression of feed efficiency within a pedigree male broiler line: I. Highlight on mitochondria, PLoS One 11 (2016) e0155679, https://doi.org/10.1371/JOURNAL.PONE.0155679.
[12] N. Sato, T. Taniguchi, Y. Goda, H. Kosaka, K. Higashino, T. Sakai, et al., Proteomic analysis of human tendon and ligament: solubilization and analysis of insoluble extracellular matrix in connective tissues, J. Proteome Res. 15 (2016) 4709–4721, https://doi.org/10.1021/ACS.JPROTEOME.6B00806/ASSET/IMAGES/LARGE/PR-2016-00806A_0004.JPEG.
[13] C.Y.C. Yeung, A.T. Olesen, R. Wilson, S.R. Lamandé, J.F. Bateman, R.B. Svensson, et al., Proteome profiles of intramuscular connective tissue: influence of aging and physical training, J. Appl. Physiol. 134 (2023) 1278–1286, https://doi.org/10.1152/JAPPLPHYSIOL.00675.2022/ASSET/IMAGES/LARGE/JAPPLPHYSIOL.00675.2022_F005.JPEG.
[14] C.J. Klein, J.A. Vrana, J.D. Theis, P.J. Dyck, P.J.B. Dyck, R.J. Spinner, et al., Mass spectrometric–based proteomic analysis of amyloid neuropathy type in nerve tissue, Arch. Neurol. 68 (2011) 195–199, https://doi.org/10.1001/ARCHNEUROL.2010.261.
[15] L. Suo, W. Dai, X. Chen, X. Qin, G. Li, S. Song, et al., Proteomics analysis of N-methyl-d-aspartate-induced cell death in retinal and optic nerves, J. Proteome 252 (2022) 104427, https://doi.org/10.1016/J.JPROT.2021.104427.
[16] H. Hwang, B.P. Bowen, N. Lefort, C.R. Flynn, E.A. De Filippis, C. Roberts, et al., Proteomics analysis of human skeletal muscle reveals novel abnormalities in obesity and type 2 diabetes, Diabetes 59 (2010) 33–42, https://doi.org/10.2337/DB09-0214.
[17] H. Lu, Y. Yang, E.M. Allister, N. Wijesekara, M.B. Wheeler, The identification of potential factors associated with the development of type 2 diabetes: a quantitative proteomics approach, Mol. Cell. Proteomics 7 (2008) 1434–1451, https://doi.org/10.1074/MCP.M700478-MCP200/ATTACHMENT/415B89E3-AF91-4747-AD6E-038D1ED4AD04/MMC1.PDF.
[18] T. Sundsten, H. Ortsäter, Proteomics in diabetes research, Mol. Cell. Endocrinol. 297 (2009) 93–103, https://doi.org/10.1016/J.MCE.2008.06.018.
[19] M.C.W. Gast, J.H.M. Schellens, J.H. Beijnen, Clinical proteomics in breast cancer: a review, Breast Cancer Res. Treat. 116 (2009) 17–29, https://doi.org/10.1007/S10549-008-0263-3/TABLES/2.
[20] D.P. Nusinow, J. Szpyt, M. Ghandi, C.M. Rose, E.R. McDonald, M. Kalocsay, et al., Quantitative proteomics of the cancer cell line encyclopedia, Cell 180 (2020), https://doi.org/10.1016/J.CELL.2019.12.023 (387-402.e16).
[21] P.R. Srinivas, M. Verma, Y. Zhao, S. Srivastava, Proteomics for cancer biomarker discovery, Clin. Chem. 48 (2002) 1160–1169, https://doi.org/10.1093/CLINCHEM/48.8.1160.
[22] Q. Fu, J.E. Van Eyk, Proteomics and heart disease: identifying biomarkers of clinical utility, Expert Rev. Proteomics 3 (2006) 237–249, https://doi.org/10.1586/14789450.3.2.237.
[23] E. McGregor, M.J. Dunn, Proteomics of heart disease, Hum. Mol. Genet. 12 (2003) R135–R144, https://doi.org/10.1093/HMG/DDG278.
[24] H. Sun, D. Wang, D. Liu, Z. Guo, C. Shao, W. Sun, et al., Differential urinary proteins to diagnose coronary heart disease based on iTRAQ quantitative proteomics, Anal. Bioanal. Chem. 411 (2019) 2273–2282, https://doi.org/10.1007/S00216-019-01668-7/FIGURES/4.
[25] R.M. Boteanu, V.I. Suica, L. Ivan, F. Safciuc, E. Uyy, E. Dragan, et al., Proteomics of regenerated tissue in response to a titanium implant with a bioactive surface in a rat tibial defect model, Sci. Rep. 10 (2020), https://doi.org/10.1038/S41598-020-75527-2.
[26] E. Calciolari, N. Mardas, X. Dereka, A.K. Anagnostopoulos, G.T. Tsangaris, N. Donos, The effect of experimental osteoporosis on bone regeneration: part 2, proteomics results, Clin. Oral Implants Res. 28 (2017) e135–e145, https://doi.org/10.1111/CLR.12950.
[27] A.I. Hussein, C. Mancini, K.E. Lybrand, M.E. Cooke, H.E. Matheny, B.L. Hogue, et al., Serum proteomic assessment of the progression of fracture healing, J. Orthop. Res. 36 (2018) 1153–1163, https://doi.org/10.1002/JOR.23754.
[28] H.Y. Yang, J. Kwon, M.S. Kook, S.S. Kang, S.E. Kim, S. Sohn, et al., Proteomic analysis of gingival tissue and alveolar bone during alveolar bone healing, Mol. Cell. Proteomics 12 (2013) 2674–2688, https://doi.org/10.1074/mcp.M112.026740.
[29] Y. Förster, J.R. Schmidt, D.K. Wissenbach, S.E.M. Pfeiffer, S. Baumann, L. C. Hofbauer, et al., Microdialysis sampling from wound fluids enables quantitative assessment of cytokines, proteins, and metabolites reveals bone defect-specific molecular profiles, PLoS One 11 (2016) e0159580, https://doi.org/10.1371/JOURNAL.PONE.0159580.
[30] E. Calciolari, N. Donos, Proteomic and transcriptomic approaches for studying bone regeneration in health and systemically compromised conditions, Proteomics Clin. Appl. 14 (2020), https://doi.org/10.1002/PRCA.201900084.
[31] E. Borgiani, C. Figge, B. Kruck, B.M. Willie, G.N. Duda, S. Checa, Age-related changes in the mechanical regulation of bone healing are explained by altered cellular mechanoresponse, J. Bone Miner. Res. 34 (2019), https://doi.org/10.1002/jbmr.3801.
[32] S. Checa, P.J. Prendergast, G.N. Duda, Inter-species investigation of the mechano-regulation of bone healing: comparison of secondary bone healing in sheep and rat, J. Biomech. 44 (2011), https://doi.org/10.1016/j.jbiomech.2011.02.074.
[33] M. Jaber, L.C. Hofbauer, C. Hofbauer, G.N. Duda, S. Checa, Reduced bone regeneration in rats with type 2 diabetes mellitus as a result of impaired stromal cell and osteoblast function—a computer modeling study, JBMR Plus 7 (2023) e10809, https://doi.org/10.1002/JBM4.10809.
[34] M. Jaber, P.S.P. Poh, G.N. Duda, S. Checa, PCL strut-like scaffolds appear superior to gyroid in terms of bone regeneration within a long bone large defect: an in silico study, Front. Bioeng. Biotechnol. 10 (2022) 995266, https://doi.org/10.3389/fbioe.2022.995266.
[35] C. Perier-Metz, G.N. Duda, S. Checa, Mechano-biological computer model of scaffold-supported bone regeneration: effect of bone graft and scaffold structure on large bone defect tissue patterning, Front. Bioeng. Biotechnol. 8 (2020), https://doi.org/10.3389/fbioe.2020.585799.
[36] P.J. Prendergast, R. Huiskes, K. Søballe, Biophysical stimuli on cells during tissue differentiation at implant interfaces, J. Biomech. 30 (1997) 539–548, https://doi.org/10.1016/S0021-9290(96)00140-6.
[37] D. Lacroix, P.J. Prendergast, G. Li, D. Marsh, Biomechanical model to simulate tissue differentiation and bone regeneration: application to fracture healing, Med. Biol. Eng. Comput. 40 (2002), https://doi.org/10.1007/BF02347690.
[38] D. Lacroix, P.J. Prendergast, A mechano-regulation model for tissue differentiation during fracture healing: analysis of gap size and loading, J. Biomech. 35 (2002), https://doi.org/10.1016/S0021-9290(02)00086-6.
[39] E. Borgiani, G. Duda, B. Willie, S. Checa, Bone healing in mice: does it follow generic mechano-regulation rules? Facta Univ. Ser. Mech. Eng. 13 (2015) 217–227. Available at: http://casopisi.junis.ni.ac.rs/index.php/FUMechEng/article/view/1395. (Accessed 19 January 2024).
[40] K.J. Jepsen, B. Hu, S.M. Tommasini, H.-W. Courtland, C. Price, C.J. Terranova, et al., Genetic randomization reveals functional relationships among morphologic and tissue-quality traits that contribute to bone strength and fragility, Mamm. Genome 18 (2007) 492–507, https://doi.org/10.1007/s00335-007-9017-5.
[41] K. Lybrand, B. Bragdon, L. Gerstenfeld, Mouse models of bone healing: fracture, marrow ablation, and distraction osteogenesis, Curr. Protoc. Mouse Biol. 5 (2015) 35–49, https://doi.org/10.1002/9780470942390.mo140161.
[42] T. Wehner, U. Wolfram, T. Henzler, F. Niemeyer, L. Claes, U. Simon, Internal forces and moments in the femur of the rat during gait, J. Biomech. 43 (2010), https://doi.org/10.1016/j.jbiomech.2010.05.028.
[43] A. Carlier, L. Geris, J. Lammens, H. Van Oosterwyck, Bringing computational models of bone regeneration to the clinic, Wiley Interdiscip. Rev. Syst. Biol. Med. 7 (2015) 183–194, https://doi.org/10.1002/WSBM.1299.
[44] L. Podshivalov, A. Fischer, P.Z. Bar-Yoseph, On the road to personalized medicine: multiscale computational modeling of bone tissue, Arch. Comput. Methods Eng. 21 (2014) 399–479, https://doi.org/10.1007/S11831-014-9120-1/FIGURES/84.
[45] A. Corti, M. Colombo, J.M. Rozowsky, S. Casarin, Y. He, D. Carbonaro, et al., A predictive multiscale model of in-stent restenosis in femoral arteries: linking haemodynamics and gene expression with an agent-based model of cellular dynamics, J. R. Soc. Interface 19 (2022), https://doi.org/10.1098/RSIF.2021.0871.
[46] M. Ponce-de-Leon, A. Montagud, V. Noël, A. Meert, G. Pradas, E. Barillot, et al., PhysiBoSS 2.0: a sustainable integration of stochastic Boolean and agent-based modelling frameworks, npj Syst. Biol. Appl. 91 (9) (2023) 1–12, https://doi.org/10.1038/s41540-023-00314-4.
[47] J. Retzlaff, X. Lai, C. Berking, J. Vera, Integration of transcriptomics data into agent-based models of solid tumor metastasis, Comput. Struct. Biotechnol. J. 21 (2023) 1930–1941, https://doi.org/10.1016/J.CSBJ.2023.02.014.
[48] S. Zhang, A. Deshpande, B.K. Verma, H. Wang, H. Mi, W. Jin Ho, et al., Informing Virtual Clinical Trials of Hepatocellular Carcinoma With Spatial Multi-Omics Analysis of a Human Neoadjuvant Immunotherapy Clinical Trial, 2023, https://doi.org/10.1101/2023.08.11.553000.
[49] J. McCauley, A. Walsh, J.F. Bejar, J. Ianni, M. Georges, Z. Zachwieja, et al., A Meta-analysis of immune signaling pathways between human type 2 diabetic tissue and mouse bone repair, Biomed. Res. Clin. Pract. 5 (2020), https://doi.org/10.15761/BRCP.1000202.

[50] E. Calciolari, S. Hamlet, S. Ivanovski, N. Donos, Pro-osteogenic properties of hydrophilic and hydrophobic titanium surfaces: crosstalk between signalling pathways in in vivo models, J. Periodontal Res. 53 (2018) 598–609, https://doi.org/10.1111/JRE.12550.
[51] S. Wang, J. Deng, S. Yuan, Q. Lu, X. Gu, C. Huang, S. Guo, D. Yu, X. Yin, Transcriptomic Analysis of Ipsilateral Spinal Cord in Rats After Bone Fracture, 2023, https://doi.org/10.21203/RS.3.RS-2782796/V1.
[52] Y. Deng, N. Luo, M. Xie, L. He, R. Jiang, N. Hu, et al., Transcriptome landscape comparison of periodontium in developmental and renewal stages, Front. Endocrinol. (Lausanne) 14 (2023) 1154931, https://doi.org/10.3389/FENDO.2023.1154931/BIBTEX.
[53] A. Ramser, R. Hawken, E. Greene, R. Okimoto, B. Flack, C.J. Christopher, et al., Bone metabolite profile differs between normal and femur head necrosis (FHN/BCO)-affected broilers: implications for dysregulated metabolic cascades in FHN pathophysiology, Metabolites 13 (2023) 662, https://doi.org/10.3390/METABO13050662.
[54] S. Hozain, A. Hernandez, J. Fuller, G. Sharp, J. Cottrell, Zinc chloride affects chondrogenesis via VEGF signaling, Exp. Cell Res. 399 (2021) 112436, https://doi.org/10.1016/J.YEXCR.2020.112436.
[55] F. Abd Rahman, Gene expression profiling on effect of aspirin on osteogenic differentiation of periodontal ligament stem cells, BDJ Open 71 (7) (2021) 1–10, https://doi.org/10.1038/s41405-021-00090-5.
[56] L.M. Luttrell, M.S. Dar, D. Gesty-Palmer, H.M. El-Shewy, K.M. Robinson, C. J. Haycraft, et al., Transcriptomic characterization of signaling pathways associated with osteoblastic differentiation of MC-3T3E1 cells, PLoS One 14 (2019) e0204197, https://doi.org/10.1371/JOURNAL.PONE.0204197.
[57] M. Bionaz, E. Monaco, M.B. Wheeler, Transcription adaptation during in vitro adipogenesis and osteogenesis of porcine mesenchymal stem cells: dynamics of pathways, biological processes, up-stream regulators, and gene networks, PLoS One 10 (2015) e0137644, https://doi.org/10.1371/JOURNAL.PONE.0137644.
[58] N. Orlando, G. Babini, P. Chiusolo, C.G. Valentini, V. De Stefano, L. Teofili, Pre-exposure to defibrotide prevents endothelial cell activation by lipopolysaccharide: an ingenuity pathway analysis, Front. Immunol. 11 (2020) 585519, https://doi.org/10.3389/FIMMU.2020.585519/BIBTEX.
[59] K.A. Morio, R.H. Sternowski, E. Zeng, K.A. Brogden, Antimicrobial peptides and biomarkers induced by ultraviolet irradiation have the potential to reduce endodontic inflammation and facilitate tissue healing, Pharmaceutics 14 (2022) 1979, https://doi.org/10.3390/PHARMACEUTICS14091979/S1.
[60] A. Alshammari, F. Alabdah, W. Wang, G. Cooper, Virtual design of 3D-printed bone tissue engineered scaffold shape using mechanobiological modeling: relationship of scaffold pore architecture to bone tissue formation, Polymers (Basel) 15 (2023), https://doi.org/10.3390/polym15193918.
[61] L.E. Claes, C.A. Heigele, Magnitudes of local stress and strain along bony surfaces predict the course and type of fracture healing, J. Biomech. 32 (1999) 255–266, https://doi.org/10.1016/S0021-9290(98)00153-5.
[62] H. Isaksson, C.C. van Donkellar, R. Huiskes, K. Ito, Corroboration of mechanoregulatory algorithms for tissue differentiation during fracture healing: comparison with in vivo results, J. Orthop. Res. 24 (2006) 898–907, https://doi.org/10.1002/JOR.20118.
[63] H. Isaksson, W. Wilson, C.C. van Donkelaar, R. Huiskes, K. Ito, Comparison of biophysical stimuli for mechano-regulation of tissue differentiation during fracture healing, J. Biomech. 39 (2006) 1507–1516, https://doi.org/10.1016/J.JBIOMECH.2005.01.037.
[64] M. Steiner, L. Claes, A. Ignatius, F. Niemeyer, U. Simon, T. Wehner, Prediction of fracture healing under axial loading, shear loading and bending is possible using distortional and dilatational strains as determining mechanical stimuli, J. R. Soc. Interface 10 (2013), https://doi.org/10.1098/RSIF.2013.0389.
[65] A. Vetter, F. Witt, O. Sander, G.N. Duda, R. Weinkamer, The spatio-temporal arrangement of different tissues during bone healing as a result of simple mechanobiological rules, Biomech. Model. Mechanobiol. 11 (2012), https://doi.org/10.1007/s10237-011-0299-x.
[66] M. Wang, N. Yang, Three-dimensional computational model simulating the fracture healing process with both biphasic poroelastic finite element analysis and fuzzy logic control, Sci. Rep. 8 (2018) 6744, https://doi.org/10.1038/s41598-018-25229-7.
[67] L.N.M. Hayward, C.M.J. de Bakker, H. Lusic, L.C. Gerstenfeld, M.W. Grinstaff, E.F. I. Morgan, MRT letter: contrast-enhanced computed tomographic imaging of soft callus formation in fracture healing, Microsc. Res. Tech. 75 (2012) 7–14, https://doi.org/10.1002/JEMT.21100.
[68] K.J. Jepsen, C. Price, L.J. Silkman, F.H. Nicholls, P. Nasser, B. Hu, et al., Genetic variation in the patterns of skeletal progenitor cell differentiation and progression during endochondral bone formation affects the rate of fracture healing, J. Bone Miner. Res. 23 (2008) 1204–1216, https://doi.org/10.1359/JBMR.080317.
[69] I.H. Borai, N.S. Hassan, O.G. Shaker, E. Ashour, M.E. Badrawy, O.M. Fawzi, et al., Synergistic effect of ACE and AGT genes in coronary artery disease, Beni-Suef Univ. J. Basic Appl. Sci. 7 (2018) 111–117, https://doi.org/10.1016/j.bjbas.2017.09.003.
[70] A.V. Chervonsky, Y. Wang, F.S. Wong, I. Visintin, R.A. Flavell, C.A.J. Janeway, et al., The role of Fas in autoimmune diabetes, Cell 89 (1997) 17–24, https://doi.org/10.1016/s0092-8674(00)80178-6.
[71] V. Locatelli, V.E. Bianchi, Effect of GH/IGF-1 on bone metabolism and osteoporsosis, Int. J. Endocrinol. 2014 (2014) 235060, https://doi.org/10.1155/2014/235060.
[72] M. Olivier, M. Hollstein, P. Hainaut, TP53 mutations in human cancers: origins, consequences, and clinical use, Cold Spring Harb. Perspect. Biol. 2 (2010) a001008, https://doi.org/10.1101/cshperspect.a001008.
[73] B. Wirostko, T.Y. Wong, R. Simó, Vascular endothelial growth factor and diabetic complications, Prog. Retin. Eye Res. 27 (2008) 608–621, https://doi.org/10.1016/j.preteyeres.2008.09.002.
[74] M. Shibuya, Vascular endothelial growth factor (VEGF) and its receptor (VEGFR) signaling in angiogenesis: a crucial target for anti- and pro-angiogenic therapies, Genes Cancer 2 (2011) 1097–1105, https://doi.org/10.1177/1947601911423031.
[75] E.K. Simmons, Characterization of the microstructural properties that are predictive of regain in strength in phosphate-deficient mice, Available at: https://open.bu.edu/handle/2144/17050, 2016.
[76] K.R. O'Neill, C.M. Stutz, N.A. Mignemi, M.C. Burns, M.R. Murry, J.S. Nyman, et al., Micro-computed tomography assessment of the progression of fracture healing in mice, Bone 50 (2012) 1357–1367, https://doi.org/10.1016/j.bone.2012.03.008.
[77] K.E. Pelch, S.M. Carleton, C.L. Phillips, S.C. Nagel, Developmental exposure to xenoestrogens at low doses alters femur length and tensile strength in adult mice, Biol. Reprod. 86 (2012) 69, https://doi.org/10.1095/biolreprod.111.096545.
[78] N.P. Camacho, C.M. Rimnac, R.A.J. Meyer, S. Doty, A.L. Boskey, Effect of abnormal mineralization on the mechanical behavior of X-linked hypophosphatemic mice femora, Bone 17 (1995) 271–278, https://doi.org/10.1016/8756-3282(95)00210-5.
[79] B. Kruck, E.A. Zimmermann, S. Damerow, C. Figge, C. Julien, D. Wulsten, et al., Sclerostin neutralizing antibody treatment enhances bone formation but does not rescue mechanically induced delayed healing, J. Bone Miner. Res. Off. J. Am. Soc. Bone Miner. Res. 33 (2018) 1686–1697, https://doi.org/10.1002/jbmr.3454.
[80] J.H. Holstein, M.D. Menger, U. Culemann, C. Meier, T. Pohlemann, Development of a locking femur nail for mice, J. Biomech. 40 (2007) 215–219, https://doi.org/10.1016/j.jbiomech.2005.10.034.
[81] M.D. Brodt, C.B. Ellis, M.J. Silva, Growing C57Bl/6 mice increase whole bone mechanical properties by increasing geometric and material properties, J. Bone Miner. Res. Off. J. Am. Soc. Bone Miner. Res. 14 (1999) 2159–2166, https://doi.org/10.1359/jbmr.1999.14.12.2159.
[82] C.H. Joo, H. Lee, E. Kim, B. Lee, Y.K. Cho, Y.K. Kim, Differential amplifying RT-PCR: a novel RT-PCR method to differentiate mRNA from its DNA lacking intron, J. Virol. Methods 100 (1-2) (2002) 71–81, https://doi.org/10.1016/s0166-0934(01)00401-3. PMID: 11742654.